Spin-resolved elastic scattering of electrons from sodium

S.R. Lorentz, R.E. Scholten, J.J. McClelland, M.H. Kelley, and R.J. Celotta
Electron and Optical Physics Division, National Institute of Standards and Technology, Gaithersburg, Maryland 20899
(Received 5 November 1992)

Angle-resolved ratios of the separate triplet and singlet spin channel cross sections have been measured for elastic scattering of spin-polarized electrons from optically pumped spin-polarized sodium atoms. The triplet-to-singlet ratios are reported at incident energies of 4.1, 10.0, and 20.0 eV for scattering angles from 20° to 140°. The data demonstrate that spin-exchange scattering plays an important role in the description of electron scattering from sodium at these energies. Comparisons are made with the results of several close-coupling theoretical calculations.

PACS number(s): 34.80.Nz, 34.80.Bm

I. INTRODUCTION

Interactions between electrons and atoms play an important role in many complex physical processes of interest, for example, in stellar plasmas, upper atmosphere chemistry, gas lasers, and semiconductor devices. To understand and model these processes with anything more than an empirical approach requires detailed knowledge of the underlying electron-atom scattering behavior. Scattering parameters, which characterize the interactions in terms of readily measurable quantities (typically electron-atom collision cross sections), are therefore needed for a large and diverse variety of systems, and for many of these it has been necessary to rely on theoretical predictions. These predictions are founded on approximations which have been tested by comparison of theoretical and experimental results from several key collision systems. The comparisons have been made using total and differential cross sections, or at a greater level of detail using scattering parameters which describe the alignment and orientation of the atom after the collision [1–3]. Ultimately, theoretical calculations can be considered reliable only if they successfully predict all quantum observables, including the electron spin [4].

Technological advances in the past two decades now enable the production of spin-polarized electron and atom beams, which provide the means to experimentally study the role of spin in electron-atom scattering. Investigations of spin-orbit effects at high energy, or equivalently using high-Z targets, have probed relativistic aspects of the collision problem [5]. Scattering of low-energy spin-polarized electrons from spin-polarized low-Z, one-electron target atoms has allowed direct measurement of spin exchange by providing the means to differentiate between triplet and singlet scattering cross sections [6–11].

While hydrogen would seem to be the ideal prototypical target, experimental difficulties have limited its use to a few spin-resolved investigations [8]. Alkali metals, on the other hand, have been the focus of considerable theoretical and experimental effort in electron-atom scattering. Alkali metals are attractive from a theoretical perspective, with their relatively simple hydrogenlike electronic structure. They are also good candidates for close-coupling calculations due to their strong coupling between the ground and first excited states. In sodium, for example, these states alone account for 99% of the static dipole polarizability [12]. Sodium is also a light atom, and therefore spin-orbit effects can be neglected for low scattering energies. Experimentally, sodium is convenient due to both the moderate oven temperatures required for producing beams, and the ease of optical pumping since the $3S$-$3P$ transition closely coincides with the peak wavelength of the robust laser dye Rhodamine 6G.

Previous spin-resolved investigations of elastic electron–alkali-metal scattering have investigated a number of different alkali-metal species. Collins, Bederson, and Goldstein [6] reported results for potassium using the recoil method at incident energies of 0.5–1.2 eV with unpolarized electrons on polarized atoms, measuring the polarization of the potassium after scattering. Hils *et al.* [7] studied potassium employing a crossed-beam method, measuring the atomic polarization after scattering unpolarized electrons from polarized atoms at an incident energy of 3.3 eV, and scattering angles from 20° to 120°.

Several experiments have also been carried out with both incident electrons and target atoms spin polarized. Fletcher *et al.* [8] made measurements on hydrogen at several incident energies from 4 to 30 eV at the fixed scattering angle of 90°. In lithium, Baum *et al.* [9] reported results at three fixed angles for incident energies from 1 to 30 eV. Results for sodium have been reported in McClelland, Kelley, and Celotta [10] at incident energies of 54.4 eV and more recently [11] at 4.1 and 12.1 eV for the angular range 20° to 135°. In Lorentz *et al.* [13] results for energies of 1.0 and 1.6 eV (i.e., below the first-excited-state threshold) are provided for a similar range of angles.

In this paper we report the measurement of angle-resolved spin channel ratios for elastic electron-sodium scattering at 4.1, 10, and 20 eV. Data are presented over a wide angular range from 20° to 140° at 5° intervals. The

energies were chosen to correspond to existing [14, 15] spin-resolved superelastic ($3P$-$3S$) results at the equivalent incident energies of 2.0, 7.9, and 17.9 eV. The measurements provide data for comparison with theoretical calculations both above and below the ionization potential of sodium at 5.14 eV.

II. EXPERIMENT

Figure 1 is a schematic of the experimental arrangement, showing the four main components: polarized electron source, electron detector, sodium oven, and laser. The scattering plane is defined by the incident and scattered electron trajectories. The electrons are spin polarized with spins aligned up or down in the laboratory reference frame and perpendicular to the scattering plane. The atoms are also spin polarized up or down, parallel to the optical pumping laser which is again perpendicular to the plane.

Electrons that scatter from the atoms through a given scattering angle $\theta_{\rm scat}$ are detected with a channel electron multiplier after passing through a retarding field analyzer to discriminate against inelastic events. The post-collisional electron and atom spins are not resolved.

At each energy and scattering angle, four spin-dependent intensities are recorded: with initial electron and atom spins parallel up $I^{\uparrow\uparrow}$, parallel down $I^{\downarrow\downarrow}$, antiparallel up $I^{\uparrow\downarrow}$, and antiparallel down $I^{\downarrow\uparrow}$. The first arrow indicates electron spin and the second the atomic spin. The intensities are then combined to form the spin exchange asymmetry

$$A_{\rm ex} = \frac{1}{P_e P_a} \frac{(I^{\uparrow\downarrow} + I^{\downarrow\uparrow}) - (I^{\uparrow\uparrow} + I^{\downarrow\downarrow})}{(I^{\uparrow\downarrow} + I^{\downarrow\uparrow}) + (I^{\uparrow\uparrow} + I^{\downarrow\downarrow})} \quad (1)$$

$$= \frac{|S|^2 - |T|^2}{|S|^2 + 3|T|^2}, \quad (2)$$

where P_e and P_a are the polarizations of the electron and atom beams, respectively, and S and T are the singlet and triplet complex scattering amplitudes. The exchange asymmetry can range from $+1$ in the case of pure singlet scattering to $-1/3$ for pure triplet scattering.

Note that the parallel intensities $I^{\downarrow\downarrow}$ and $I^{\uparrow\uparrow}$ are averaged, as are the antiparallel intensities $I^{\uparrow\downarrow}$ and $I^{\downarrow\uparrow}$. In the absence of relativistic effects such as spin-orbit interactions there is symmetry with respect to reflection in the scattering plane, and this averaging serves to eliminate any possible systematic asymmetry between "up" and "down" in the laboratory reference frame. Spin-orbit effects can also be extracted from the same four intensities [16], but these were found to be negligible for sodium at the collision energies measured.

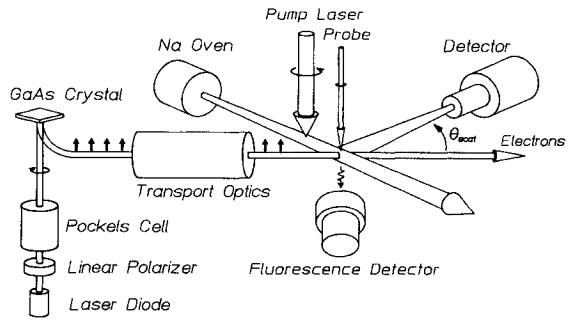

FIG. 1. Experimental configuration, showing polarized electron source, electron detector, oven, laser, and fluorescence monitor.

The experimental results are presented here as the ratio of triplet to singlet cross sections $r = |T|^2/|S|^2$, which can be expressed in terms of the exchange asymmetry of Eq. (2) as

$$r = \frac{1 - A_{\rm ex}}{1 + 3A_{\rm ex}}. \quad (3)$$

III. APPARATUS

The major components of the apparatus depicted in Fig. 1 have been described in an earlier paper [14], so only those aspects specific to the current experiments deserve further elaboration. In particular, the optical pumping arrangement has been enhanced with the addition of an acousto-optic modulator to enable simultaneous pumping of two transitions [17], and is therefore discussed separately in Sec. IV.

The electron beam was produced by photoemission from a negative electron affinity GaAs crystal [18] at currents ranging from 1.0 to 2.5 μA as the energy was varied from 4.1 to 20 eV. The electron beam energy calibration and width were determined by measuring the helium $1s2s^2\ ^2S$ resonance at 19.36 eV [19]. The scattering chamber was filled with helium to a pressure of 1.6×10^{-5} Pa (1.2×10^{-7} Torr), and elastically scattered electrons were detected at 90° while the electron energy was ramped from 19 to 20 eV. This measurement provides both an absolute scale for the electron energy, and the energy width of the electron beam (250 ± 50 meV full width at half maximum).

The electron energy calibration was further tested by measuring the optical excitation function of the $3S$-$3P$ transition in sodium. A photomultiplier was used to detect fluorescence resulting from electronic excitations at the electron/sodium interaction region as the energy of the electron beam was swept from 1.5 to 2.5 eV. The acquired optical excitation function allows a determination of the energy calibration and width of the electron beam at 2.1 eV, the first excited state of sodium. The results thus obtained proved consistent with those of the helium resonance measurement at 19.36 eV.

The polarization of the electron beam P_e was measured to be 0.32 ± 0.02 using a 100 keV cylindrical Mott analyzer [20]. The uncertainty in the electron polarization is due primarily to the inherent calibration uncertainties associated with Mott polarimetry measurements [21, 22].

IV. OPTICAL PUMPING

The atomic beam was polarized to 0.987 ± 0.007 by optically pumping the $3S_{1/2} \rightarrow 3P_{3/2}$ (D_2) transition using

a single-mode stabilized ring dye laser. An acousto-optic modulator was used to generate a second, frequency-shifted beam so that both ground-state hyperfine levels are involved in the pumping process. The pumping scheme relies on circularly polarized light to excite transitions with $\Delta M_F = \pm 1$ (Fig. 2). Repeated cycles of excitation followed by decay through spontaneous emission result in a net migration of the population of the sublevels towards higher M_F for σ^+ or lower M_F for σ^- pumping.

If all the atoms are allowed to decay to the ground state, the atomic polarization with quantization axis parallel to the pumping laser beam, P_A, is given by

$$P_A = \left[\rho_{\overline{22}} + \frac{1}{2}\rho_{\overline{21}} - \frac{1}{2}\rho_{\overline{2-1}} - \rho_{\overline{2-2}}\right] + \left[\frac{1}{2}\rho_{\overline{1-1}} - \frac{1}{2}\rho_{\overline{11}}\right], \tag{4}$$

where ρ_{FM} is the normalized population of the FM_F sublevel. Initially, the atoms are in thermal equilibrium, with all $\overline{M}_F$ substates equally populated. Thus 5/8 of the atoms are in the $\overline{F} = 2$ state, and 3/8 in $\overline{F} = 1$, and $P_A = 0$.

Assuming single-frequency pumping at the $\overline{F} = 2 \rightarrow F = 3$ transition, and σ^+ polarization, the $\overline{F} = 2$ atoms ideally all reach the $\overline{F} = 2, \overline{M}_F = 2$ ground state and $F = 3, M_F = 3$ excited state levels from which they cannot escape. The $\overline{F} = 1$ states are separated from the $\overline{F} = 2$ states by about 1.7 GHz and are therefore inaccessible to the pumping process. Hence only 5/8 of the initial atoms are pumped, and the atomic polarization has a maximum value of 5/8 or 62.5%.

With single-frequency pumping, several factors can reduce the atomic polarization below the expected 62.5%. The finite natural linewidth of 10 MHz, and more significantly the saturated linewidth [23], result in some

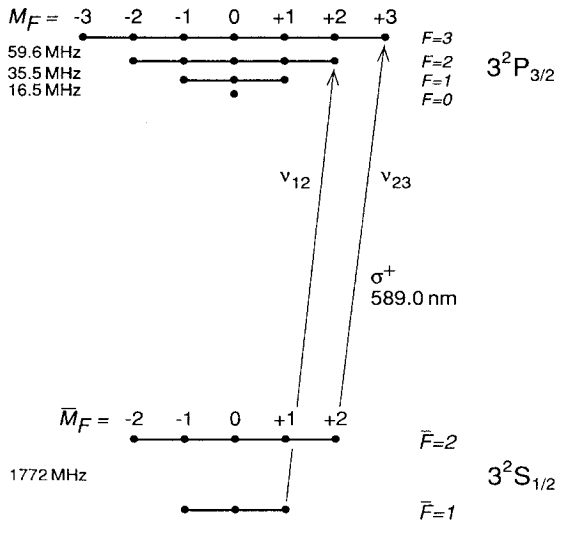

FIG. 2. Sodium energy levels showing pumping lines ν_{23} and $\nu_{12} = \nu_{23} + 1712$ MHz. By common convention, ground states are distinguished from excited states by an overbar, for example, $\overline{F}$.

overlap of the desired $\overline{F} = 2 \rightarrow F = 3$ and undesired $\overline{F} = 2 \rightarrow F = 2$ transitions. Atoms excited to the $F = 2$ state can decay to the unpumped $\overline{F} = 1$ ground-state hyperfine level. These atoms are then trapped and do not experience the polarizing effect of the optical pumping process [24].

Further depolarization can be caused by stray magnetic fields. The spin of a sodium atom with a velocity of 1000 m s^{-1} along a magnetic field will precess through an angle of approximately 10° nT^{-1} m^{-1} (10° mG^{-1}cm^{-1}), which corresponds to a loss of approximately 1.5% of the atomic polarization for a 0.1 μT (1 mG) field over a distance of 1 cm. This was minimized by enclosing the scattering chamber in a triple-layer magnetic shield which attenuated the ambient magnetic field to less than 0.1 μT. The effects of precession were also reduced by pumping close to the interaction region, while still providing sufficient distance for the majority of atoms to decay to the ground state. A separation of 2 mm has been used so that depolarization is less than 0.1% while still allowing 120 lifetimes for the atoms to decay.

In order to increase the atomic polarization it is necessary to access those atoms in the $\overline{F} = 1$ state. This can be accomplished by pumping with two frequencies corresponding to both the "normal" $\overline{F} = 2 \rightarrow F = 3$ transition and to the otherwise unpumped $\overline{F} = 1 \rightarrow F = 2$ transition. This requires either two lasers [25], or a single laser with an electro-optic modulator [26] or an acousto-optic modulator (AOM) [17].

The AOM has several advantages, including commercial availability at the desired $\overline{F} = 1$ to 2 modulation frequency of 1712 MHz, and spatial separation of the fundamental and frequency-shifted components. This separation necessitates additional optics which must be carefully aligned to ensure optimum pumping at both frequencies, but permits use of either component as a separate "probe" beam which can be used to analyze the atomic polarization outside the main pumping region.

The dye laser output at the $\overline{F} = 2 \rightarrow F = 3$ frequency (ν_{23}) was focused into the AO crystal and collimated afterwards with $f = 50$ mm antireflection-coated spherical lenses. The frequency-shifted $\overline{F} = 1 \rightarrow F = 2$ component (ν_{12}) was diffracted by about 5°. This beam was reflected from a mirror placed close to the AOM and collimated with the same lens as that used for the fundamental, and then reflected with a mirror after the lens so as to converge with the fundamental at the pumping region approximately 5 m away. This arrangement was chosen to minimize the separation angle (0.06°) between the two beams, ensuring that they are both incident on the atom beam at close to the ideal 90°. Total throughput of better than 50% was obtained with approximately equal intensities, typically 150–200 mW, in each beam.

The atomic polarization was determined by measuring and analyzing the fluorescence induced by a low-intensity probe beam incident perpendicular to the scattering plane. The fluorescence was detected using a lens, linear polarizer, and photomultiplier located in the scattering plane. A gap of approximately 2 mm separated the probe, centered on the interaction region, and the pump region upstream (i.e., towards the oven), to allow com-

plete decay of the excited atoms. The measured atomic polarization was therefore that relevant to the scattering process. Investigation of residual magnetic fields was also possible by moving the probe beam and measuring depolarization of the fluorescence with distance from the pump region.

The atomic polarization depends on the magnetic sublevel population distribution of both the $\overline{F} = 1$ and $\overline{F} = 2$ states. Using the two-frequency pumping scheme, the $\overline{F} = 1$ population should be only a small fraction of the total. This was verified by measuring the fluorescence $\mathcal{F}_{12}$ of a weak probe beam tuned to the ν_{12} transition with the pump beams on and off, so that

$$\rho_{\overline{F}=1} = \frac{3}{8}\frac{\mathcal{F}_{12}\ \text{(pump on)}}{\mathcal{F}_{12}\ \text{(pump off)}}. \tag{5}$$

In practice, when pumping with two frequencies the $\overline{F} = 1$ population was never larger than 0.4%, and this effect on the final atomic polarization has been ignored.

The atomic polarization can then be determined from the population distribution among the $\overline{F} = 2$ magnetic sublevels. While it is possible to measure the separate magnetic sublevel populations definitively, using magnetic fields to Zeeman split the magnetic sublevels, these magnetic fields cause difficulties with low-energy electron scattering experiments and also lead to precession of the atomic spin. Instead, we have used an analysis of the polarization of the fluorescence, detected at 90° to a circularly polarized probe tuned to the ν_{23} transition frequency, together with optimistic and pessimistic models of the pumping behavior.

For a σ^+ circularly polarized probe, the detected linear polarization P_L is related to the ground-state populations by (see Appendix)

$$P_L = \frac{9\rho_{\overline{2}\overline{-2}} + 36\rho_{\overline{2}\overline{-1}} + 54\rho_{\overline{20}} - 225\rho_{\overline{22}}}{23\rho_{\overline{2}\overline{-2}} + 72\rho_{\overline{2}\overline{-1}} + 138\rho_{\overline{20}} + 200\rho_{\overline{21}} + 225\rho_{\overline{22}}}. \tag{6}$$

Note that P_L will be negative for circular pumping.

Clearly from Eqs. (6) and (4) it is not possible to absolutely determine the atomic polarization simply from a measurement of P_L. Instead, two models of the expected magnetic sublevel distribution have been used to relate the fluorescence polarization to an atomic polarization. First there is the optimistic model, which presumes that all those atoms not in the desired $\rho_{\overline{22}}$ state will be in its neighbor $\rho_{\overline{21}}$ state (Fig. 3, upper inset). That is, $\rho_{\overline{2}\overline{-2}} = \rho_{\overline{2}\overline{-1}} = \rho_{\overline{20}} = 0$; $\rho_{\overline{21}} \equiv \epsilon$ and $\rho_{\overline{22}} = 1 - \epsilon$. This presumes that the σ^+ pumping tends to push the atoms to higher M_F. Given this, using Eqs. (4) and (6) the atomic polarization would be

$$P_A = \frac{1}{2} - \frac{4P_L}{9 + P_L}. \tag{7}$$

The second model is far more pessimistic, and assumes that those atoms not in the desired $\rho_{\overline{22}}$ state are evenly distributed among the $\overline{F} = 2, \overline{M}_F = -2, -1, 0$, and 1 sublevels (Fig. 3, lower inset). That is, $\rho_{\overline{2}\overline{-2}} = \rho_{\overline{2}\overline{-1}} = \rho_{\overline{20}} = \rho_{\overline{21}} \equiv \epsilon/4$ and $\rho_{\overline{22}} = 1 - \epsilon$. The pessimistic prediction then gives an atomic polarization of

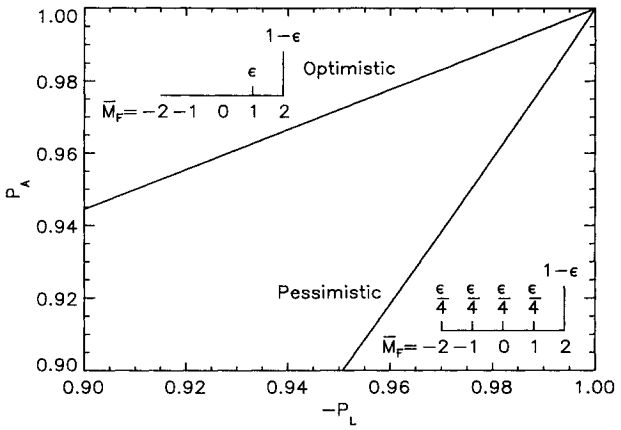

FIG. 3. Atomic polarization P_A vs fluorescence polarization P_L for the optimistic and pessimistic models. The insets show the magnetic sublevel population distributions for the $\overline{F} = 2$ ground state assumed by the two models.

$$P_A = \frac{-(126 + 658\,P_L)}{999 + 467\,P_L}. \tag{8}$$

Figure 3 shows the results for P_A vs P_L for the two models. Given a typical pump laser intensity of $50\,\text{mW cm}^{-2}$ in each pump beam, the measured fluorescence polarization was -0.990 or better, indicating an atomic polarization perpendicular to the scattering plane of $P_A = 0.987 \pm 0.007$. This value is the average between the optimistic and pessimistic models, with uncertainty taken as the limits of these two models.

V. EXPERIMENTAL PROCEDURE

The four scattering intensities $I^{\uparrow\uparrow}$, $I^{\downarrow\downarrow}$, $I^{\uparrow\downarrow}$, and $I^{\downarrow\uparrow}$ were obtained by counting scattered electrons as the spins of the target atoms and the incident electrons were modulated. The electron spin polarization was flipped at 100 Hz by application of a high voltage square wave to a Pockels cell reversing the helicity of the light inducing photoemission from the GaAs. The atom spin polarization was reversed every 1–5 sec by switching the helicity of the optical pumping light. This was accomplished by mechanically rotating a zero-order quarter-wave plate which was mounted following a Glan-Thompson linear polarizer. In order to measure the background electron count rate, the sodium beam was shuttered every 1–5 sec by moving a paddle to block the exit aperture of the sodium oven. The data reported here are the result of one to four hours of total collection time per point.

The error bars shown in the figures were derived from the propagation of the uncertainty due to counting statistics through the expression for the ratio, and are plotted only where larger than the symbols used to represent the data points. The systematic uncertainties in the atom and electron polarizations P_e and P_A are not included, since these polarizations remain essentially constant from one scattering angle to another, and therefore the uncer-

tainty in the combined polarization $P = P_e P_A$ affects only the scale of the ratio axis. For absolute comparisons with theory and with other experimental results, this uncertainty in scale can be calculated from a scaling factor given by

$$f = \frac{\delta + 4r + 3r\delta}{r(4 + \delta + 3r\delta)}, \tag{9}$$

where $\delta = dP/P$ is the uncertainty in polarization; in our case $P = 0.316$ and $\delta = \pm 0.07$. The upper and lower systematic limits of a given data point r are then given by fr, where f depends on r and δ, and on the sign of δ. The total uncertainty on the data point would be the quadrature sum of the systematic and statistical uncertainties. The systematic uncertainty is separated in this way because, once a given value of δ is chosen so as to bring theory and experiment into agreement, at one energy and angle, that same value of δ must be used at *all* energies and angles. The relative uncertainty between data points is statistical only.

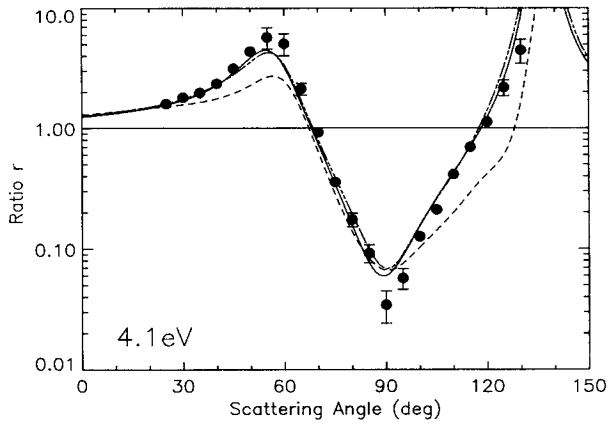

FIG. 4. Triplet-to-singlet ratio r for elastic electron–sodium scattering vs scattering angle at 4.1 eV incident energy. •, present results; —, Bray and McCarthy [29]; – – –, Moores and Norcross [12]; – · · –, Zhou, Whitten, and Norcross [27].

VI. RESULTS AND DISCUSSION

Figures 4–6 show the triplet-to-singlet ratio r plotted on a log scale, for incident energies of 4.1, 10, and 20 eV. The 4.1 and 10 eV measurements show a pronounced singlet dominance, around 90° and 60°, respectively. The relative importance of triplet and singlet channels varies dramatically, in fact by three orders of magnitude at 10 eV where triplet accounts for 80% of the cross section at 45° and only 1% at 60°.

The effects of spin are much less apparent at 20 eV, and previous measurements at 54.4 eV [10] support the trend towards smaller exchange effects at higher energies. This is expected since exchange is essentially the result of the Pauli exclusion principle acting between the incident and bound electrons; as the energy increases the de Broglie wavelength of the incident electron becomes smaller, and thus the overlap of the incident and bound electronic wave functions is reduced. This model is overly simplistic, but provides some indication of the energy-dependent behavior.

Figures 4–6 also show the results of several theoretical calculations based on the close-coupling approximation. The close-coupling approach should be successful for sodium even if only a few low-lying states are included since the excitation to the $3P$ state accounts for approximately 99% of the ground-state static dipolarizability.

Moores and Norcross [12] and Zhou, Whitten, and Norcross [27] have solved the close-coupling equations with four- and ten-state expansions, respectively, although solutions were restricted to low energies. Mitroy, McCarthy, and Stelbovics [28] used four states at higher energies, including 10 and 20 eV. Bray and McCarthy [29] have recently extended the close-coupling method to fifteen states, including coupling through higher discrete states and the continuum for the first six states using an optical potential.

At 4.1 eV all three calculations predict the general features of the triplet-to-singlet ratio against scattering angle. The ten-state close coupling (10CC) results of Zhou, Whitten, and Norcross and the fifteen-state (15CCO6) results of Bray and McCarthy are almost identical, both showing exceptional agreement with the experimental values. The Moores-Norcross calculation, which only includes four states, is less successful near the maximum at about 60° and again at larger angles beyond the minimum at 90°. The sophistication required, that is, the large number of states which must be treated explicitly in the close-coupling expansion, is surprising given the very strong coupling between the ground and first excited states in sodium. Bray and McCarthy note that fifteen states were necessary for convergence at 4.1 eV.

A comparatively large number of states are also beneficial at higher energies. The four-state close-coupling (4CC) results of Mitroy, McCarthy, and Stelbovics predict the general behavior observed at 10 eV but again the 15CCO6 calculation more accurately reproduces

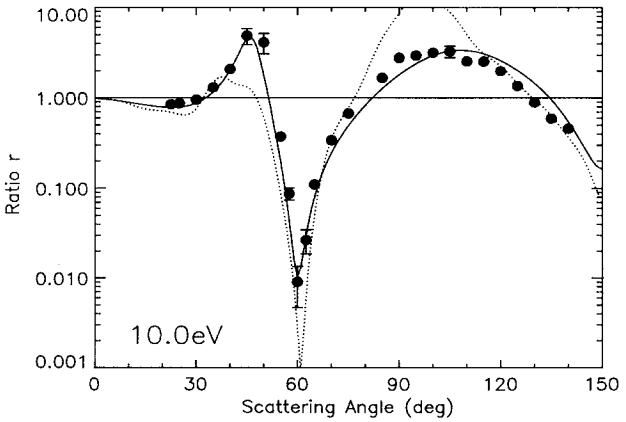

FIG. 5. Triplet-to-singlet ratio r for elastic electron–sodium scattering vs scattering angle at 10 eV incident energy. •, present results; —, Bray and McCarthy [29]; · · ·, Mitroy, McCarthy, and Stelbovics [28].

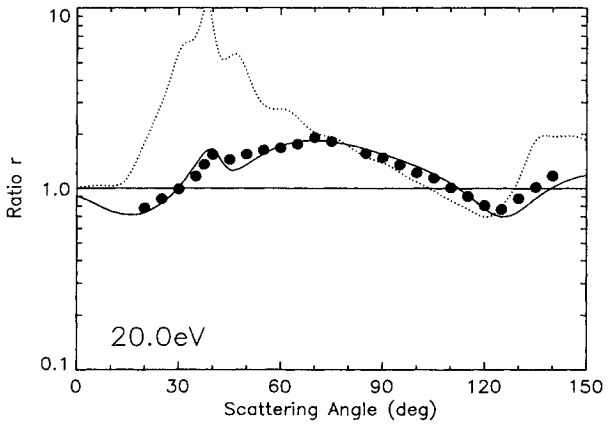

FIG. 6. Triplet-to-singlet ratio r for elastic electron–sodium scattering vs scattering angle at 20 eV incident energy. •, present results; —, Bray and McCarthy [29]; · · · Mitroy, McCarthy, and Stelbovics [28].

the measured triplet-to-singlet scattering ratio. The 15CCO6 theory is also very successful at 20 eV, especially when compared to the earlier 4CC model. While the strong coupling in sodium led Mitroy, McCarthy, and Stelbovics to conclude that an optical potential was unnecessary, comparison based on these spin-resolved experiments, which probe theory in considerable detail, clearly justifies the extended calculations of Bray and McCarthy.

VII. CONCLUSIONS

The data given here complete an extensive series of spin-resolved electron scattering measurements from sodium. Triplet-to-singlet scattering channel ratios have been measured at 4.1, 10, and 20 eV, that is, above and below the 5.14 eV ionization potential of sodium. In conjunction with previous elastic measurements at 1.0, 1.6, 12.1, and 54.4 eV [10, 11, 13] and inelastic $3S$-$3P$ studies at 4.1, 10, 20, and 40 eV [14, 15] they provide a solid basis for comparison with various theoretical approaches to calculation of electron-atom scattering phenomena.

Theoreticians have traditionally relied on cross-section measurements to test their results, but unfortunately such parameters average two or more calculated scattering amplitudes. It has been possible to find apparent agreement between theory and experimental measurements which later experiments having greater specificity show to be coincidental. The ratio of triplet-to-singlet scattering amplitudes is fundamental, and has the additional advantage of being a relative measurement and therefore insensitive to many experimental factors which are difficult to control. Hence accurate prediction of experimental ratios is a stringent test of theoretical models.

The latest theoretical results show excellent agreement with the experimental values given here, at all energies measured. Predictions of exchange effects have in the past been less successful at energies of 20 eV and above, but the increased number of coupled states and the inclusion of an optical potential to account for the target continuum in the theory of Bray and McCarthy have apparently resolved these problems.

ACKNOWLEDGMENT

This work is supported in part by the U.S. Department of Energy, Office of Energy Research, Division of Chemical Sciences.

APPENDIX

The linear polarization of fluorescence from a circularly polarized probe beam was used to estimate the ground-state magnetic sublevel population distribution and thereby the atomic polarization. This fluorescence polarization is defined as

$$P_L = \frac{\mathcal{F}_\parallel - \mathcal{F}_\perp}{\mathcal{F}_\parallel + \mathcal{F}_\perp}, \tag{A1}$$

where $\mathcal{F}_\parallel$ and $\mathcal{F}_\perp$ are the fluorescence intensities detected at 90° to the probe beam and with polarization parallel and perpendicular to the plane defined by the probe and detector axes respectively.

Writing ρ_{FM_F} as the normalized population of the FM_F excited-state sublevel and $A_{\overline{FM}_F FM_F}$ as the transition rate for decay from the FM_F excited state to the $\overline{FM}_F$ ground state, the relative fluorescence intensities are given by

$$\mathcal{F}_\parallel = \sum_{M=-3}^{+3} A_{2M3M}\,\rho_{3M} \qquad (\Delta M = 0 \text{ decay}), \tag{A2}$$

$$\mathcal{F}_\perp = \underbrace{\frac{1}{2}\sum_{M=-3}^{+3} A_{2(M-1)3M}\,\rho_{3M}}_{\Delta M=-1} + \underbrace{\frac{1}{2}\sum_{M=-3}^{+3} A_{2(M+1)3M}\rho_{3M}}_{\Delta M=+1}, \tag{A3}$$

where the factor of 1/2 in the $\mathcal{F}_\perp$ term comes from the different spatial dipole radiation distribution patterns for circular versus linear transitions [30].

The excited-state populations ρ_{3M_F} can be written in terms of equivalent ground-state populations $\rho_{\overline{2M}_F}$, assuming a weak purely circularly polarized probe beam:

$$\rho_{3M} = B_{2(M\pm1)3M}\,\rho_{\overline{2}(M\pm1)} \tag{A4}$$

for $\sigma^\mp$ probes. This assumes that the probe beam has sufficiently low intensity that optical pumping effects of the probe can be neglected. The transition rates for sodium, in which decay to two ground states with different angular momenta is possible, are given by

$$A_{\overline{F}\overline{M}_F F M_F} = \frac{1}{\tau}\,(2F+1)(2\overline{F}+1)(2J+1)(2\overline{J}+1)(2L+1)\begin{pmatrix}\overline{F} & F & 1\\ \overline{M}_F & -M_F & q\end{pmatrix}^2\begin{Bmatrix}\overline{J} & \overline{F} & I\\ F & J & 1\end{Bmatrix}^2\begin{Bmatrix}\overline{L} & \overline{J} & S\\ J & L & 1\end{Bmatrix}^2,$$

$$B_{\overline{F}\overline{M}_F F M_F} = \frac{3\lambda}{4h}A_{\overline{F}\overline{M}_F F M_F},$$

where q is the polarization ($q = M_F - \overline{M}_F$), $I = 3/2$ is the nuclear moment, $J = 3/2$ and $\overline{J} = 1/2$, $\overline{L} = 0$ and $L = 1$, $S = 1/2$, and τ is the lifetime. Given these transition rates it is then straightforward to substitute Eqs. (A2) and (A3) into Eq. (A1) to arrive at Eq. (6).

[1] M. Eminyan, K.B. MacAdam, J. Slevin, and H. Kleinpoppen, J. Phys. B **31**, 576 (1973).
[2] M.C. Standage and H. Kleinpoppen, Phys. Rev. Lett. **36**, 577 (1976).
[3] N. Andersen, J.W. Gallagher, and I.V. Hertel, Phys. Rep. **165**, 1 (1988).
[4] B. Bederson, Comments At. Mol. Phys. **1**, 41 (1969).
[5] O. Berger and J. Kessler, Phys. Rev. Lett. **45**, 768 (1981).
[6] R.E. Collins, B. Bederson, and M. Goldstein, Phys. Rev. A **3**, 1976 (1971).
[7] D. Hils, M.V. McCusker, H. Kleinpoppen, and S.J. Smith, Phys. Rev. Lett. **29**, 398 (1972).
[8] G.D. Fletcher, M.J. Alguard, T.J. Gay, V.W. Hughes, C.W. Tu, P.F. Wainwright, M.S. Lubell, W. Raith, and F.C. Tang, Phys. Rev. Lett. **48**, 1671 (1982).
[9] G. Baum, M. Moede, W. Raith, and U. Sillmen, Phys. Rev. Lett. **57**, 1855 (1986).
[10] J.J. McClelland, M.H. Kelley, and R.J. Celotta, Phys. Rev. Lett. **58**, 2198 (1987).
[11] J.J. McClelland, S.R. Lorentz, R.E. Scholten, M.H. Kelley, and R.J. Celotta, Phys. Rev. A **46**, 6079 (1992).
[12] D.L. Moores and D.W. Norcross, J. Phys. B **5**, 1482 (1972).
[13] S.R. Lorentz, R.E. Scholten, J.J. McClelland, M.H. Kelley, and R.J. Celotta, Phys. Rev. Lett. **67**, 3761 (1991).
[14] J.J. McClelland, M.H. Kelley, and R.J. Celotta, Phys. Rev. A **40**, 2321 (1989).
[15] R.E. Scholten, S.R. Lorentz, J.J. McClelland, M.H. Kelley, and R.J. Celotta, J. Phys. B **24**, L653 (1991).
[16] J.J. McClelland, S.J. Buckman, M.H. Kelley, and R.J. Celotta, J. Phys. B **23**, L21 (1990).
[17] G. Baum, C. D. Caldwell, and W. Schröder, Appl. Phys. **21**, 121 (1980).
[18] D.T. Pierce, R.J. Celotta, G.C. Wang, W.N. Unertl, A. Galejs, C.E. Kuyatt, and S.R. Mielczarek, Rev. Sci. Instrum. **51**, 478 (1980).
[19] L. Sanche and G.J. Schulz, Phys. Rev. A **5**, 1672 (1972).
[20] L.A. Hodge, T.J. Moravec, F.B. Dunning, and G.K. Walters, Rev. Sci. Instrum. **50**, 5 (1979).
[21] G.D. Fletcher, T.J. Gay, and M.S. Lubell, Phys. Rev. A **34**, 911 (1986).
[22] A. Gellrich, K. Jost, and J. Kessler, Rev. Sci. Instrum. **61**, 3399 (1990).
[23] L. Allen and J.H. Eberly, *Optical Resonance and Two-Level Atoms* (Wiley, New York, 1975).
[24] J.J. McClelland and M.H. Kelley, Phys. Rev. A **31**, 3704 (1985).
[25] W. Dreves, W. Kamke, W. Broermann, and D. Fick, Z. Phys. A **303**, 203 (1981).
[26] J.F. Kelly and A. Gallagher, Rev. Sci. Instrum. **58**, 563 (1987).
[27] H.L. Zhou, B.L. Whitten, and D.W. Norcross, Bull. Am. Phys. Soc. **36**, 1283 (1991).
[28] J. Mitroy, I.E. McCarthy, and A. Stelbovics, J. Phys. B **20**, 4827 (1987). Results for unpublished parameters and energies provided by private communication.
[29] I. Bray and I.E. McCarthy, Phys. Rev. A **47**, 317 (1993).
[30] E.U. Condon and G.H. Shortley, *The Theory of Atomic Spectra* (Cambridge University Press, Cambridge, 1951).